The influenza fusion peptide promotes lipid polar head intrusion through hydrogen bonding with phosphates and N-terminal membrane insertion depth

ARTICLE *in* PROTEINS STRUCTURE FUNCTION AND BIOINFORMATICS · SEPTEMBER 2014

Impact Factor: 2.63 · DOI: 10.1002/prot.24568 · Source: PubMed

2 AUTHORS:

Sébastien Légaré
Laval University
3 PUBLICATIONS **10** CITATIONS
SEE PROFILE

Patrick Lagüe
Laval University
34 PUBLICATIONS **396** CITATIONS
SEE PROFILE

PROTEINS
STRUCTURE ■ FUNCTION ■ BIOINFORMATICS

The influenza fusion peptide promotes lipid polar head intrusion through hydrogen bonding with phosphates and N-terminal membrane insertion depth

Sébastien Légaré and Patrick Lagüe*

Département de Biochimie, Microbiologie et Bio-informatique, Institut de Biologie Intégrative et des Systèmes (IBIS), Centre de Recherche sur la Fonction, la Structure et l'ingénierie des Protéines (PROTEO), Université Laval, Quebec City, Quebec, Canada

ABSTRACT

Influenza infection requires fusion between the virus envelope and a host cell endosomal membrane. The influenza hemagglutinin fusion peptide (FP) is essential to viral membrane fusion. It was recently proposed that FPs would fuse membranes by increasing lipid tail protrusion, a membrane fusion transition state. The details of how FPs induce lipid tail protrusion, however, remain to be elucidated. To decipher the molecular mechanism by which FPs promote lipid tail protrusion, we performed molecular dynamics simulations of the wild-type (WT) FP, fusogenic mutant F9A, and nonfusogenic mutant W14A in model bilayers. This article presents the peptide–lipid interaction responsible for lipid tail protrusion and a related lipid perturbation, polar head intrusion, where polar heads are sunk under the membrane surface. The backbone amides from the four N-terminal peptide residues, deeply inserted in the membrane, promoted both perturbations through H bonding with lipid phosphates. Polar head intrusion correlated with peptides N-terminal insertion depth and activity: the N-termini of WT and F9A were inserted deeper into the membrane than nonfusogenic W14A. Based on these results, we propose that FP-induced polar head intrusion would complement lipid tail protrusion in catalyzing membrane fusion by reducing repulsions between juxtaposed membranes headgroups. The presented model provides a framework for further research on membrane fusion and influenza antivirals.

Proteins 2014; 82:2118–2127.

Key words: membrane peptide; lipid mixing; lipid polar head intrusion; lipid tail protrusion; membrane fusion; peptide N-terminus-lipid phosphate H bond.

INTRODUCTION

The influenza virus binds to host cell surface receptors, is endocytosed, and fuses its viral envelope with the endosomal membrane in response to reduced pH.[1–3] The binding and membrane fusion steps are mediated by the hemagglutinin (HA), a glycoprotein embedded in the viral membrane. HA is a homotrimer and each monomer is composed of two disulfide-bound subunits.[4] Endosomal acidification triggers a conformational change in HA2, the second subunit, which is responsible for membrane fusion through a spring-loaded mechanism.[5] Although the entire HA2 subunit participates in membrane fusion, the 20 N-terminal residues, which compose the fusion peptide (FP) domain, are the only parts of HA that insert into the endosomal membrane during the fusion process[6] (see Refs. 2 and 5 for a detailed picture of the FP domain and HA2 conformational changes during fusion process). It has been shown that FPs that are not attached to HA induce lipid mixing,[7–10] but require the complete HA[11] or polyethylene glycol[12] to complete the fusion process. Hence, FPs alone catalyze the formation of membrane fusion intermediate states such as the stalk and hemifusion.

The molecular mechanism by which FPs promote lipid mixing between two juxtaposed membranes remains to

Additional Supporting Information may be found in the online version of this article.

Grant sponsor: Canada Foundation for Innovation (CFI); Grant sponsor: National Science and Engineering Research Council (NSERC); Grant sponsor: PROTEO (S. L.).
*Correspondence to: Patrick Lagüe; Département de Biochimie, Microbiologie et Bio-informatique, Pavillon Charles-Eugène-Marchand, 1030, avenue de la Médecine, Université Laval, Quebec City, QC, Canada G1V 0A6.
E-mail: Patrick.Lague@bcm.ulaval.ca
Received 30 October 2013; Revised 3 March 2014; Accepted 19 March 2014
Published online 26 March 2014 in Wiley Online Library (wileyonlinelibrary.com). DOI: 10.1002/prot.24568

be elucidated. Although many FP-induced membrane perturbations associated with fusion have been proposed such as membrane thinning,[13–15] membrane curvature,[14,16] changes in lipid order, [14,17–19] and lipid tilting,[20] they are insufficient to generate a comprehensive molecular model for lipid mixing catalysis. It is indeed not clear how these perturbations can establish a localized hydrophobic contact between bilayers to initiate stalk formation.[21] Molecular dynamics (MD) simulations have revealed that protrusion of lipid hydrophobic tails at the membrane surface may be the transition state for fusion stalk formation.[21–25] and that lipid tail protrusion is higher in the vicinity of FPs.[24,25] Interestingly, a comparison of the X-31 influenza strain with the G1V and G1S mutants showed that peptides promote lipid tail protrusion in proportion to the ability of the corresponding full-length HA to drive lipid mixing in fusion assays.[25] Although a correlation between lipid tail protrusion and fusogenic activities was observed, it is not known how peptides promote lipid tail protrusion. An understanding of this process would improve the development of membrane fusion inhibitors with the ability to prevent influenza infections.[26–28]

To decipher the molecular mechanism by which FPs promote lipid tail protrusion, we performed MD simulations of the wild-type (WT) FP, fusogenic mutant F9A, and nonfusogenic mutant W14A[29,30] in model bilayers. We identified the peptide–lipid interaction responsible for protrusion and a related lipid perturbation (lipid polar head intrusion) for which the polar head is sunk into the membrane. We compared WT and mutant-induced perturbations to show that polar head intrusion was correlated to fusogenic activity.

This article first presents the regions of higher probabilities of lipid tail protrusion and polar head intrusion around the WT FP, and the F9A and W14A mutants. The molecular mechanism by which the peptides promote tail protrusion and head intrusion is then described. Finally, a model for FP-induced lipid mixing is proposed. The model is general in nature and may also explain the activities of viral fusogenic tilted peptides.[31] The details of the MD simulations and the trajectory analysis are provided in the METHODS section.

METHODS

Simulations

Type 3 HA FP from influenza virus strain X-31 with the WT GLFGA-IAGFI-ENGWE-GMIDG sequence and the F9A and W14A mutants were studied in 1-palmitoyl-2-oleoyl-sn-glycero-3-phosphocholine (POPC) membranes from MD simulations. Choice of starting conformations, systems building, and simulations were made following the same methodology as used in our previous studies of the FP structure and dynamics.[32] Briefly, four FP conformations were selected from Protein Data Bank (PDB) entry 1IBN[33] and were used to generate starting conformations for the three peptides. The mutant peptides were built by replacing residues F9 and W14 by alanines with internal coordinates from CHARMM topology.[34] The peptides were inserted at the lipid/water interface of model POPC membranes following EPR-determined membrane topology,[32] that is, the C_α of N12 at the average position of the lipid phosphate groups and an angle of 37° with the bilayer plane for the N-terminal helix formed by residues 2–10, using previously described methods.[35–37] The systems were simulated in a cubic unit cell of ~64 Å each side, and were composed of approximately 28,000 atoms: 123 lipids (64 for the lower leaflet and 59 for the upper, where the peptide stands), 30 water molecules for each lipid, 10 Cl^- ions, and 13 Na^+ ions. For each peptide, eight 200-ns trajectories were produced, for a total of 24 trajectories. Of the eight simulations, four were started with the structures from PDB, whereas the other four were started with the final structures of the first four WT simulations. Additionally, two 200-ns simulations of a pure POPC membrane of the same dimensions were produced to calculate bulk probabilities of lipid tail protrusion and polar head intrusion.

The simulations were performed with the NAMD2 program[38] using the CHARMM27r force field[39] with the CMAP correction,[40] TIP3P waters,[41,42] and revised tryptophan parameters.[43] Isothermal-isobaric ensemble and periodic boundary conditions were used. For each trajectory, the peptide was held fixed for the first 10 ns, and the first 50 ns were considered as equilibration time and discarded from analysis. Peptide root-mean-square deviations (RMSDs) were well stabilized after those initial 50 ns as shown on Supporting Information Figures S1–S3.

Trajectory analysis

The last 150 ns of each trajectory was used for the analyses, for a total of 1.2 μs of equilibrated sampling for each peptide. The results were averaged over 50-ns blocks, and standard errors were calculated from these averages. Lipid tail protrusion was defined as any aliphatic carbon protruding beyond its phosphate group. Polar head intrusion was defined, for a given monolayer, as any choline nitrogen atom that sinks under or equal to the average level of the phosphate groups in the monolayer. Probabilities of carbon protrusion and head intrusion shown in Table I were calculated as the average number of protruding carbons and intruding cholines, divided by the number of lipids and given as percentages.

The plots in Figures 1, 3, and 5 were obtained by first aligning the N-terminal helix of the peptides, allowing only rotations around the membrane normal to keep the membrane on the same plane for every frame. The

Table I
Protrusion and Intrusion Statistics for Pure Membranes and at the N-Terminus of the Three Peptides

System	HB occurence	Carbon protrusion[b]	Overall carbon protrusion[c]	Head intrusion[b]	Overall head intrusion[c]
Pure	–	1.1±0.1 (1)	1.1±0.1 (1)	34±1 (1.0)	34±1 (1.0)
WT[a]	50±7	19±8 (17)	11±5 (10)	63±3 (1.9)	50±3 (1.5)
F9A[a]	54±6	13±5 (11)	8±3 (7)	68±4 (2.0)	54±4 (1.6)
W14A	47±5	15±4 (13)	7±2 (6)	49±5 (1.4)	42±4 (1.2)

All values are expressed as percentage ± standard error.
Fold increase compared to bulk are in parentheses.
[a]Denotes fusogenic peptides.
[b]For lipids with H bonds with the N-termini of the peptides.
[c]For lipids with and without H bonds with the N-termini of the peptides.

membrane surface was then divided into 1-Å^2 bins. For Figure 1, the average number of phosphates belonging to lipids with at least one protruding carbon was calculated for each bin to obtain the normalized phosphate probability distributions. The average was then multiplied by the area per lipid (64 Å^2) and divided by 0.0054, the probability of finding a lipid with at least one protruding carbon in the pure membrane. The same method was used to compute the carbon distribution probabilities, except that the final division was performed using a pure membrane carbon protrusion probability of 0.011. Figure 3 was built in the same way but using intruding nitrogen atoms and their corresponding phosphates and a final division by 0.34, the pure membrane intrusion probability. For Figure 5, the average phosphate position was computed in every bin and the average number of phosphates in every bin was used to obtain phosphate density.

Carbon protrusion free energies were computed based on the ratio K of protruding and nonprotruding carbons using the equation $\Delta G = -RT\ln K$, where $T = 303.15$K and $R = 1.986\times10^{-3}$kcal K^{-1}mol^{-1}. The number of nonprotruding carbons in K was taken as the number of lipids with no protruding carbon multiplied by 2.1, that is, the average number of protruding carbons from protruding lipids in pure membranes. Head intrusion free energies were based on the ratio of intruding and nonintruding choline heads.

RESULTS AND DISCUSSION

Lipid tail protrusion

Our simulations showed that lipid tail protrusion, previously proposed as a stalk formation transition state,[24] was mostly located at the N-termini of the peptides. This precise protrusion localization was not reported in previous works.[24,25] Figure 1 (green) shows the probabilities of aliphatic carbon protrusion for lipids in peptide-containing leaflets relative to the plane of the bilayers. We observed domains of higher probability of tail protrusion in the vicinity of the three peptides. The spatial

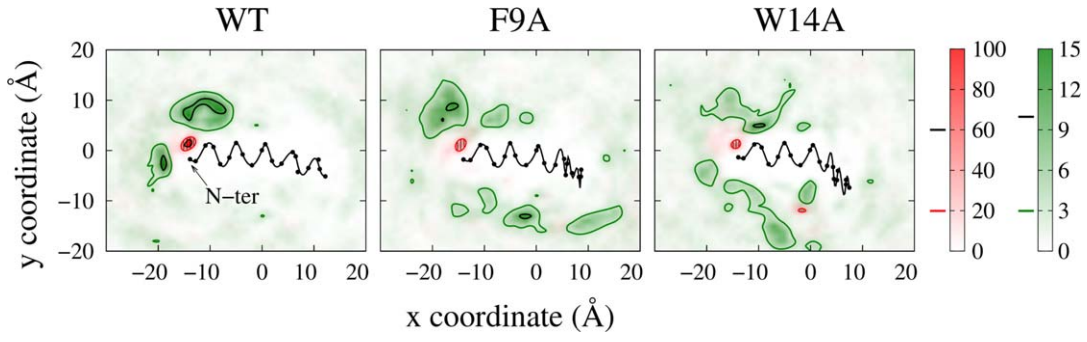

Figure 1
Normalized probability of aliphatic carbon protrusion surrounding the three peptides (green) and location of the lipid phosphates from the higher protrusion regions (red, hatched) relative to the plane of the bilayer. This is a top view of the membrane, and the x and y axis form a plane parallel to the membrane. The average C_α coordinates (black dots) represent the position of the peptides (black line). Isocontour values are indicated beside each color scale. The color scales represent the fold increase compared to the tail protrusion of a pure membrane. For carbons, the isocontours are set at 3 (green) and 10 (black). For phosphates, the isocontours are set at 20 (red) and 60 (black). Carbon probabilities are normalized relative to the average bulk probability of carbon protrusion, whereas phosphate probabilities are normalized relative to the average bulk probability of lipid protrusion. Average carbon protrusion probability for lipids away from the peptides was 1.3±0.1%, not significantly different from that of pure membranes. [Color figure can be viewed in the online issue, which is available at wileyonlinelibrary.com.]

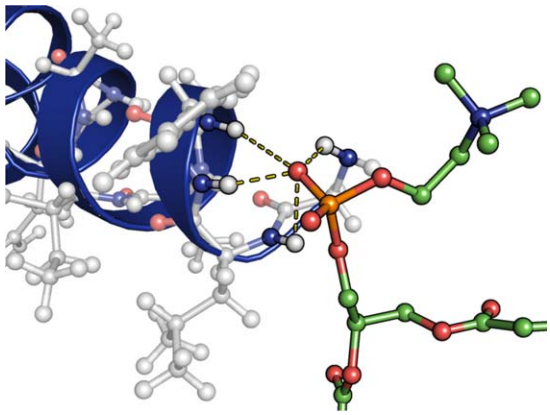

Figure 2

Typical H bonding pattern between a phosphate oxygen and the N-terminal amides of the WT peptide. Lipid hydrogens are not shown for clarity. [Color figure can be viewed in the online issue, which is available at wileyonlinelibrary.com.]

distribution of these domains was slightly different for each peptide. For the WT peptide, the increase in protrusion was confined to two domains at the N-terminus whereas F9A and W14A had few additional domains scattered around the peptides. The highest peaks were observed at the N-termini of all three peptides (Fig. 1, green). However, WT displayed a larger area for the domains of high protrusion than F9A and W14A. There was also a correlation between the spatial distribution of carbon protrusion and the flexibility of the peptides. The protrusion was more dispersed around the mutant peptides, which are more flexible than the WT peptide as reported in a previous study.[32]

The probabilities of finding a phosphate from a protruding lipid for the lipids in the peptide-containing leaflets are presented in Figure 1 (red). For the three peptides, a higher probability region (Fig. 1, red), well defined in a single domain (with a small exception for W14A) and in close contact with N-termini, was observed. The region of high concentration of phosphates from protruding lipids (Fig. 1, red) was associated with frequent hydrogen bonds between phosphates and N-terminal amides for all three peptides. The hydrogen bonds were between the phosphate oxygens and at least one of the four backbone amides of residues G1, L2, F3, and G4, as illustrated in Figure 2 for the WT. The hydrogen bonding occurrence between the N-termini of the peptides and these lipids was similar for all three peptides (see Table I) and ranged from 47 to 54% of the simulation time. To our knowledge, the peptide N-terminus-lipid phosphate H bond observed in the present work has not been reported previously. Nonetheless, solid-state NMR experiments showed that H bonding of lipid phosphates to cationic ARG and LYS side chains is important for many cell-penetrating peptides (CPP) and antimicrobial peptides (AMP) activities.[44–47] In addition, the downfield chemical shifts observed for the amide protons of residues L2 and F3[48] are consistent with such H bonding, even though these shifts might also originate from the helix dipole effects.[49]

Hydrogen bonding of lipid phosphates with the N-termini of the peptides significantly increased the probability of protrusion. Increases in carbon protrusion for lipids H bonded at the N-termini of the peptides are indicated in Table I. The probability of carbon protrusion from pure POPC membrane simulations was $1.1 \pm 0.1\%$, in good agreement with the probability found away from the FP by Larsson and Kasson.[25] The largest increase in protrusion (compared to pure membranes) was observed for the WT peptide (17-fold), followed by F9A and W14A, which increased 11- and 13-fold, respectively, although the spatial distribution for the two mutants was different. Supporting Information Figures S4–S6 show the frequencies and average times of protrusion events with respect to lipid aliphatic carbons for the lipids with and without a H bond with the peptides. These figures show that, for all three peptides, the increases in protrusion probability arose mainly from higher frequencies of oleoyl and palmitoyl chains protrusion events. The increases were more pronounced for the carbons at the beginning of both chains. For these carbons, the average time of protrusion events raised from 20 ps in the pure membrane to 40 ps for lipids H bonded to the WT N-terminus, whereas the frequency of protrusion events went from $\sim 0.08 \text{ns}^{-1}$ to $\sim 1.4 \text{ns}^{-1}$, a $\sim$17-fold increase. The average number of protruding carbons increased slightly, rising from 2.1 to 2.3–2.6 carbons per lipid in the presence of H bonding with the peptides. Protrusion in the opposite leaflet, where no peptide was inserted, was identical as in the pure membrane, and was also evenly distributed over the layer (Supporting Information Fig. S7).

Overall, when taking lipids with and without H bonds into consideration, the increase in lipid tail carbon protrusion observed at the N-termini of the peptides was higher with the WT peptide (10-fold increase) than with the mutants (seven and sixfold increases for F9A and W14A, respectively, see Table I). However, the differences between the three peptides were not statistically significant ($P > 0.05$, Kolmogorov-Smirnov test). Peptide-promoted lipid tail protrusion has been proposed to nucleate fusion stalks[24] and correlates with the fusogenic activity of the WT peptide and the G1S and G1V mutants.[25] Nevertheless, the results described above show that there is no such correlation for F9A and W14A (recall that F9A is fusogenic whereas W14A is not[29,30]).

Lipid polar head intrusion

Based on our observations of the trajectories, all the lipids that are simultaneously involved in lipid tail

protrusion and H bonding with the peptides have also their polar head (choline) significantly inserted into the membrane. The polar head nitrogens of most of these lipids were inserted into the membrane at the same level or deeper than the average position of phosphate groups, a phenomenon that we refer to as polar head intrusion. It is important to stress that polar head intrusion is defined relative to the average phosphate position of the entire lipid layer, unlike tail protrusion, which is defined relative to the position of each respective lipid phosphate (a short movie showing polar head intrusion as observed from simulations is available as Supporting Information). Furthermore, the relation between peptide-mediated lipid tail protrusion and polar head intrusion is not absolute as not all protruding lipids undergo head intrusion: 76±7%, 73±9%, and 54±10% for the WT, F9A, and W14A, respectively. On the other side very few intruding lipids experience lipid tail protrusion: 9±3%, 5±2%, and 5±2% for the WT, F9A and W14A, respectively.

As for tail protrusion, we observed a higher probability of head intrusion (Fig. 3, blue) at the N-termini of the peptides. Figure 3 (blue) shows the probability of lipid polar head intrusion for the lipids in peptide-containing leaflets. Unlike tail protrusion, the amount of head intrusion was similar for the WT and the fusogenic F9A peptides, whereas the nonfusogenic W14A peptide displayed less head intrusion. As expected, the phosphates belonging to intruding lipids from the higher probability regions were located within a single domain and were H bonded to the N-termini of the peptides (Fig. 3, red, small differences can be seen compared to what is observed for tail protrusion as not all intruding lipids undergo tail protrusion).

The probability of head intrusion from pure POPC membrane simulations was 34±1%. Hydrogen bonding of lipid phosphates to the N-termini of the peptides significantly increased the probability of polar head intrusion. The largest increases in intrusion (compared to pure membrane) were observed for the F9A mutant (twofold) and WT peptide (1.9-fold), followed by W14A (1.4-fold; Table I). Unlike lipid tail protrusion, the higher intrusion probabilities observed were the result of an increase only in the average intrusion time. The average time of intrusion events in the pure membrane was about 80 ps, and it increased to 200 ps for lipids H bonded to the WT N-terminus. The frequency of intrusion events remained close to 4 ns^{-1} in all studied conditions. In contrast to lipid tail protrusion, polar head intrusion in the opposite leaflet was slightly increased in the region under the peptide (Supporting Information Fig. S8). This result is consistent with a thinning of the membrane induced by the peptide, as reported by many previous studies.[13–15]

Overall, when taking lipids with and without H bonds into consideration, the lipid polar head intrusion observed at the N-termini of the peptides was significantly higher in the presence of WT (1.5-fold) and F9A (1.6-fold) than in the presence of W14A (1.2-fold; $P < 0.05$, Kolmogorov-Smirnov test; Table I). Our results indicate that there is a correlation between the amount of polar head intrusion induced by a peptide and the fusogenic activity of the peptide. However, the moderate difference in polar head intrusion between the WT and W14A peptides might be insufficient to explain the almost complete loss of activity of the W14A mutant. Other factors such as a weaker bilayer binding,[29] may also contribute to the nonfusogenic phenotype of the W14A mutant.

It was previously determined that tail protrusion is not increased around an ion channel, suggesting that protrusion is specific to membrane-disordering or FPs.[25] Although polar head intrusion around ion channels was not studied yet, we can presume that it will follow the same trend as tail protrusion as both perturbations are related according to our results. In addition, bilayers composed exclusively of POPC phospholipids, as used in this work, are sufficient to obtain FP-induced lipid mixing.[7] The membranes of influenza host cells also contain anionic lipids[50] that can modulate the structure and activity of FPs.[51] Vesicle content leakage experiments suggest that the presence of 1-palmitoyl-2-oleoyl-sn-glycero-3-phosphoglycerol affects the pH-dependance of the FP activity.[52] Experiments on cationic antimicrobial peptides showed that anionic lipids can change insertion depth[53] and self-association[54] of membrane active peptides. Other factors than lipid charge, like aliphatic chain length or polar head size can alter peptide insertion depth or peptide-induced membrane curvature.[54,55] However, it is expected that FP-induced increase in polar head intrusion will occur regardless of phospholipid composition as it is caused by hydrogen bonding with phosphate groups, which are part of all phospholipids. Only the amount of intrusion will vary from one bilayer composition to another.

Molecular mechanism of peptide-induced lipid conformational changes

Based on the results described above, it is clear that H bonding to the N-termini of the peptides increased the prevalence of lipid tail protrusion and polar head intrusion. However, there was no significant difference in the amount of H bonding to the three peptides. The lower levels of tail protrusion and head intrusion observed for the mutant peptides thus cannot be attributed to a decrease in the affinity of the N-termini of the mutant peptides for lipid phosphate groups. This section presents the molecular mechanism driving the peptide-induced lipid conformational change that leads to lipid tail protrusion and polar head intrusion as observed from the simulations.

Figure 4 shows two typical conformations of a lipid H bonded to the N-terminus of the WT FP. In this figure,

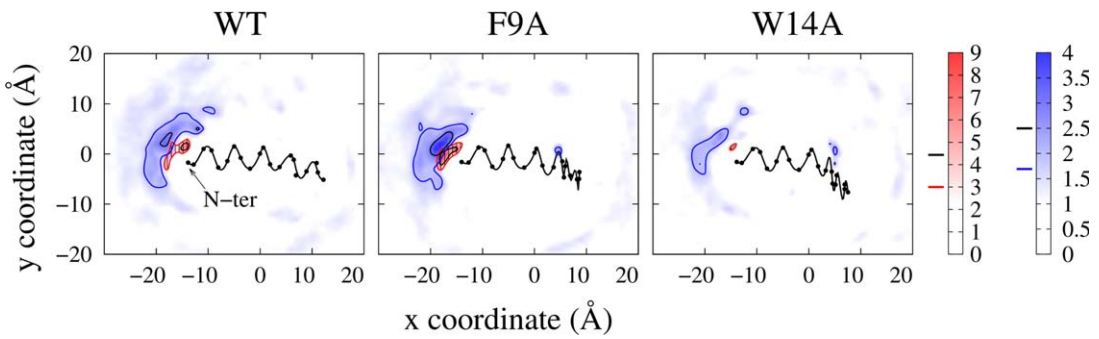

Figure 3

Normalized probability of polar head intrusion surrounding the three peptides (blue) and location of the lipid phosphates from the higher intrusion regions (red, hatched) relative to the plane of the bilayer. This is a top view of the membrane, and the *x* and *y* axes form a plane parallel to the membrane. The average C_α coordinates (black dots) represent the positions of the peptides (black line). Isocontour values are indicated beside each color scale. The color scales represent the fold increase compared to the head intrusion of a pure membrane. For polar heads (cholines), the isocontours are set at 1.7 (blue) and 2.5 (black). For phosphates, isocontours are set at 3 (red) and 4.5 (black). Probabilities are normalized relative to the average bulk probability of head intrusion. Average intrusion probability for lipids away from the peptides was 32±1%, not significantly different from that of pure membranes. [Color figure can be viewed in the online issue, which is available at wileyonlinelibrary.com.]

both the H bonded lipid phosphate and the protruding aliphatic carbons are below the average phosphate position along the bilayer normal, as represented by the red line [Fig. 4(B)]. On average, the phosphates of the protruding lipids that were H bonded to WT, F9A, and W14A were dragged 4.2 ± 0.3 Å, 4.8 ± 0.7 Å, and 3.8± 0.4 Å toward the center of the membrane, respectively. This created a membrane invagination at the N-termini of the peptides, as shown in Figure 5.

The peptides thus increased tail protrusion by dragging the lipid phosphates toward the center of the membrane, rather than by pushing the aliphatic chains up to the membrane surface. This assertion is supported by the average positions of the protruding carbons of the H bonded lipids presented in Supporting Information Figure S9. The protruding carbons were, on the average, at the same level or slightly more embedded in the membrane compared to carbons from lipids that were not H bonded.

The free energies (ΔG) of carbon protrusion were computed from the ratios of protruding versus nonprotruding carbons. The free energy of protrusion in pure membranes was 3.16±0.03 kcal/mol, whereas the values were 1.4±0.2, 1.7±0.2, and 1.6 ± 0.1 kcal/mol for lipids H bonded to WT, F9A, and W14A, respectively. All three peptides significantly lowered the free energy of lipid tail

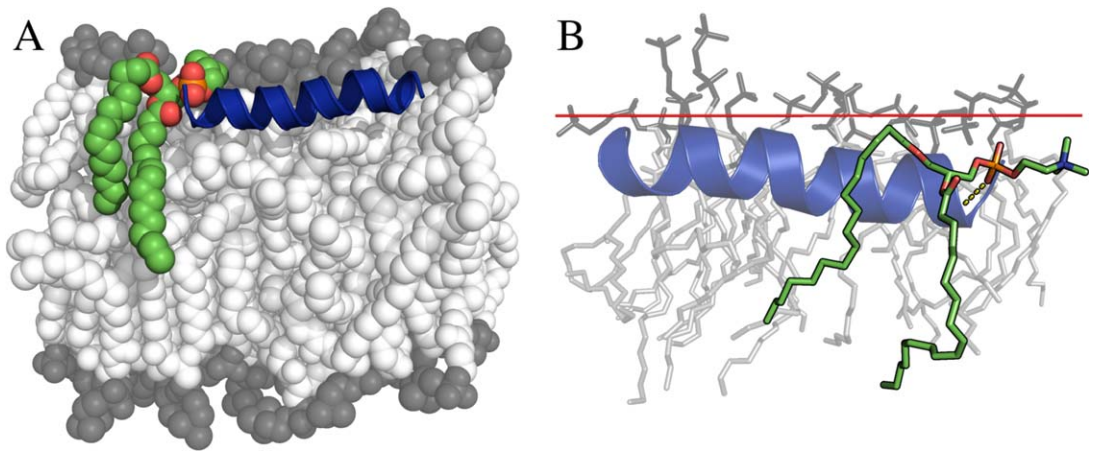

Figure 4

Two different bilayer snapshots highlighting both polar head intrusion and lipid tail protrusion for a lipid H bonded at the N-terminus of the WT FP. The FP is in blue cartoon, and membrane lipids are shown as light gray (**A**) spheres or (**B**) sticks, with polar heads in dark gray. H bonded lipids are colored by atom types with carbons in green, oxygens in red and phosphates in orange. The H bond between a peptide N-terminal amide and a phosphate oxygen represented by dashes in (B). The average position of phosphate groups from the membrane layer is represented by a red line in (B).

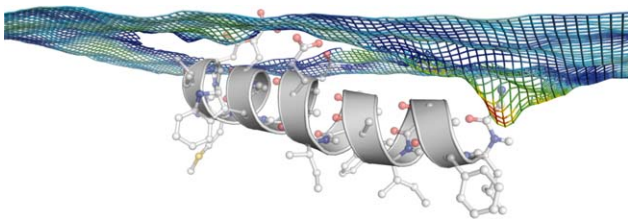

Figure 5

Membrane invagination at the WT FP N-terminus. The mesh indicates the average position of the phosphates from the membrane layer where the FP inserts. Mesh color spectrum indicate phosphate density, blue indicating a normal density and red a high density. The region of high phosphate density at the N-terminus of the FP is caused by H bonding. The FP is shown in white cartoon and sticks. [Color figure can be viewed in the online issue, which is available at wileyonlinelibrary.com.]

protrusion, with the smallest free energy being observed for the WT peptide, which was expected from the amount of protrusion described above. The protrusion free energy for pure lipids reported here is significantly higher than the value reported by Larsson et al.,[25] but is consistent with the percentage of protruding lipids observed from the simulations (Table I). Note that dragging a phosphate down leads to lipid tail protrusion as much as pushing an aliphatic chain up would according to the definition of lipid tail protrusion. However, these two perturbations may affect lipid mixing differently, as pushing an aliphatic chain up would expose aliphatic carbons at the surface of the membrane, whereas dragging a lipid phosphate down would only favor such exposure.

As a peptide drags a lipid phosphate by H bonding with its N-terminus, the choline polar head of the lipid sinks under the membrane surface. Phosphate H bonding with the N-terminus of the WT made the polar heads sink 0.8 ± 0.2 Å under the average phosphate level. The insertion depth was 1.1 ± 0.3 Å for the fusogenic F9A mutant, whereas polar heads from lipids H bonded to the nonfusogenic W14A mutant lay 0.1 ± 0.3 Å above the average phosphate level. The intrusion of lipid polar heads was stabilized by H bonding between intruding cholines and the surrounding lipid phosphates. This molecular mechanism is similar to the role played by the cationic residues ARG and LYS in CPP and AMP, for which the side chains form H bonds with lipid phosphates that favor the membrane insertion of these highly charged groups.[44–47]

The ΔG of intrusion in pure membranes was 0.40 ± 0.2 kcal/mol, which was much lower than that of lipid tail protrusion. This was expected from the relatively large amount of intrusion observed in pure membranes. Lipids H bonded to the WT, F9A, and W14A peptides had intrusion free energies of -0.33 ± 0.03, -0.46 ± 0.04, and 0.04 ± 0.06 kcal/mol, respectively. Importantly, the intrusion free energies of lipids H bonded to the N-termini of the WT and F9A peptides were significantly negative, whereas the intrusion free energy of the nonfusogenic W14A mutant remained positive.

Figure 6 presents the average backbone amide insertion depths into the membrane for the three peptides. These results show that the W14A backbone amides at the N-terminus are inserted about 0.5 Å shallower in the membrane than for WT and F9A, as was observed for the side chains in our previous study,[32] and in agreement with the experimental membrane insertions.[29] Aromatic amino acid residues were reported to be efficient anchors at the membrane interface for transmembrane proteins and peptides.[56] As a consequence, substitution of F9 or W14 by ALA increases peptide flexibility, as reported in our previous study:[32] in addition to the dominant straight α-helical and kinked conformations adopted by the WT, the mutants also visit the hairpin (F9A and W14A) and the unfolded C-terminal (W14A) conformations. As shown in Figure 6, the mutation of F9 to ALA leads to shallower membrane insertions for residues 6–20 compared to WT. In contrast, the mutation of W14 to ALA leads to the greatest flexibility among the three peptides,[32] and a shallower membrane insertion compared to WT for nearly all the residues, with the largest deviations observed at the N-terminus. These largest deviations observed for W14A come likely from the loss of H bonding between the indole amine and the lipid carbonyls which confines the residue at the membrane interface.[57] Therefore, W14A would thus drag lipid phosphates shallower under the membrane surface than the WT or F9A peptides, as confirmed by the shallower phosphate insertion depths of protruding and intruding lipids H bonded to W14A N-terminus, reported above.

In the light of our results, the decreased ability of some mutant peptides to induce lipid mixing would be

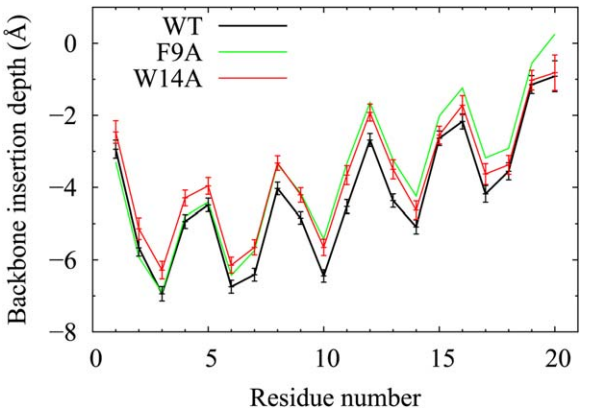

Figure 6

Depths of insertion of the peptide backbone amides under the average lipid phosphate position along the bilayer normal. [Color figure can be viewed in the online issue, which is available at wileyonlinelibrary.com.]

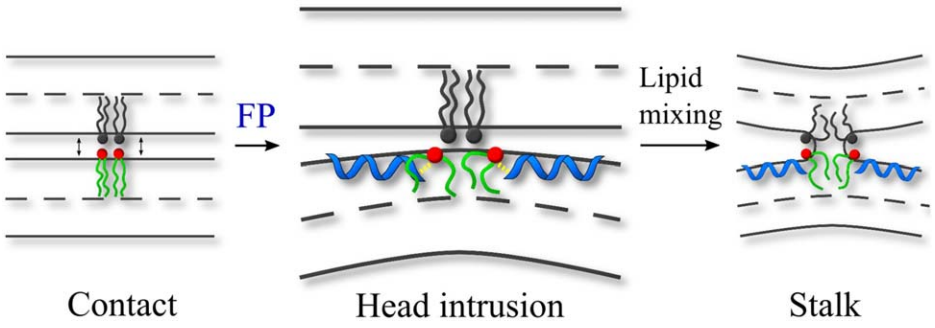

Figure 7

Proposed model for FP-catalyzed lipid mixing based on lipid head intrusion. Membranes and lipids are in black. FPs are in blue. The heads of phospholipids H bonded to the FPs are in red and the tails are in green. The H bonds between lipid phosphates and FP N-termini are indicated by yellow dashed lines. [Color figure can be viewed in the online issue, which is available at wileyonlinelibrary.com.]

caused by a smaller increase in peptide-induced polar head intrusion due to a shallower insertion of their N-termini into the membrane. The localization of important lipid perturbations at the N-termini as presented here would also concord with the strong effect of N-terminal mutations on fusogenic activity.[58,59] Based on MD trajectories, Larsson and Kasson[25] reported a lower probability of tail protrusion for the G1S and G1V peptides and suggested that this was related to their lower lipid mixing rates. Interestingly, the N-termini of the G1S and G1V mutant peptides are also less deeply inserted into the membrane than the N-terminus of the WT peptide.[15,48]

Lipid polar head intrusion and lipid mixing catalysis

Although the bilayers simulated here were too small to reproduce a complex phenomenon such as lipid mixing or membrane fusion, a speculative mechanism may be inferred from the present results. This mechanism is a complement to previously described FP-induced membrane perturbations.[13–20] To initiate lipid mixing according to the stalk hypothesis, the two membranes must first bud toward each other to create a very small region of contact.[60,61] Budding can be achieved through the membrane curvature induced by the HA[62] and FP.[14,16] Then, one must locally (1) overcome the repulsive steric-hydration and electrostatic forces and (2) create an attractive hydrophobic force at the contact region between the two membranes.[63]

We propose that polar head intrusion contributes to lipid mixing by reducing the repulsive steric-hydration and electrostatic forces between membranes. Steric-hydration and electrostatic forces are thought to be the respective sources of the short-range and long-range repulsion between juxtaposed membranes.[63,64] A steric-hydration force arise when hydrated lipid headgroups start to overlap with each other, creating a steric repulsion as two membranes approach. An electrostatic repulsion is also present between charged moieties of polar headgroups. Polar head intrusion would conceal polar headgroups under the membrane surface, hence reducing headgroup overlaps and neutralizing electrostatic charges. Simultaneously, lipid tail protrusion[24] would create an attractive hydrophobic force between the membranes by exposing aliphatic chains.

To summarize, lipid head intrusion and tail protrusion can be seen as complementary perturbations that work toward concealing polar heads and exposing lipid tails at the region of contact between membranes. Figure 7 illustrates the model of lipid mixing catalysis by FP-induced polar head intrusion. Before insertion of FPs (Fig. 7 left), the steric-hydration and electrostatic forces keep membranes from fusing. Following insertion of many FPs into the membrane (Fig. 7 middle), the packing of aliphatic chains around the FPs gives rise to a nonspecific lipid-mediated interaction that favors the clustering of FPs.[65] The curvature induced by the FPs creates a localized region of contact between the membranes. Polar head intrusion then reduces the steric-hydration and electrostatic forces in the region of contact. At the same time, lipid tail protrusion creates a hydrophobic attraction between the membranes. Polar head intrusion hence combines with previously found perturbations to form a stalk between juxtaposed membranes (Fig. 7 right).

CONCLUSIONS

We performed MD simulations of the influenza WT FP, fusogenic mutant F9A, and nonfusogenic W14A mutant in POPC membranes to investigate the molecular mechanism of FP-induced lipid tail protrusion. Lipid tail protrusion was previously proposed as a membrane fusion transition state.[21–25] Our simulations showed that tail protrusion was located at the N-termini of the peptides and was caused by hydrogen bonds between

lipid phosphates and at least one of the four N-terminal backbone amides.

Increase in polar head intrusion, a new membrane perturbation described in this work, was also observed at the N-termini of the peptides. Polar head intrusion consists in the sinking of polar head groups under the membrane surface. The increase of this perturbation was favored by hydrogen bond between the lipid phosphates and the peptide N-termini. The increases in the amount of polar head intrusion at the N-termini of the peptides correlated with fusogenic activities and N-terminal insertion depths.

We suggest that lipid polar head intrusion contributes to lipid mixing by reducing the repulsive steric-hydration and electrostatic forces between juxtaposed membranes. This perturbation would work in synergy with lipid tail protrusion that exposes aliphatic carbons at the membrane surface. Increases in head intrusion and tail protrusion are localized perturbations according to our results. Following the stalk hypothesis, fusion begins at a small contact point between the membranes.[61] A perturbation localized at the contact region could hence have a stronger effect on fusion than a membrane-wide perturbation. Although the specific interaction between phosphates and peptide N-termini observed in this work was not described previously, it is similar to the H bonding of lipid phosphates to cationic ARG and LYS side chains that has been reported to favor the membrane insertion via charge–charge neutralization.[44–47]

The proposed lipid mixing mechanism based on specific interactions between peptide N-termini and lipid phosphates may be common among fusogenic tilted peptides.[31] Our model also opens the way to further research on influenza antiviral targets. Some influenza antivirals such as arbidol may inhibit membrane fusion by binding to membranes[27] and may also decrease polar head intrusion.

ACKNOWLEDGMENT

Supercomputer time was provided by the CLUMEQ infrastructure Colosse at Université Laval.

REFERENCES

1. Weissenhorn W, Hinz A, Gaudin Y. Virus membrane fusion. FEBS Lett 2007;581:2150–2155.
2. Harrison SC. Viral membrane fusion. Nat Struct Mol Biol 2008;15: 690–698.
3. Cross KJ, Langley WA, Russell J, Skehel JJ, Steinhauer DA. Composition and functions of the influenza fusion peptide. Protein Pept Lett 2009;16:766–778.
4. Wilson IA, Skehel JJ, Wiley DC. Structure of the hemagglutinin membrane glycoprotein of influenza-virus at 3 Å resolution. Nature 1981;289:366–373.
5. Gruenke JA, Armstrong RT, Newcomb WW, Brown JC, White JM. New insights into the spring-loaded conformational change of influenza virus hemagglutinin. J Virol 2002;76:4456–4466.
6. Durrer P, Galli C, Hoenke S, Corti C, Gluck R, Vorherr T, Brunner J. H^+-induced membrane insertion of influenza virus hemagglutinin involves the HA2 amino-terminal fusion peptide but not the coiled coil region. J Biol Chem 1996;271:13417–13421.
7. Lear JD, Degrado WF. Membrane binding and conformational properties of peptides representing the NH_2 terminus of influenza HA-2. J Biol Chem 1987;262:6500–6505.
8. Murata M, Sugahara Y, Takahashi S, Ohnishi S. pH-dependent membrane-fusion activity of a synthetic 20 amino-acid peptide with the same sequence as that of the hydrophobic segment of influenza-virus hemagglutinin. J Biochem 1987;102:957–962.
9. Han X, Tamm LK. A host-guest system to study structure-function relationships of membrane fusion peptides. Proc Natl Acad Sci USA 2000;97:13097–13102.
10. Epand RM, Epand RF, Martin I, Ruysschaert JM. Membrane interactions of mutated forms of the influenza fusion peptide. Biochemistry 2001;40:8800–8807.
11. Kemble GW, Danieli T, White JM. Lipid-anchored influenza hemagglutinin promotes hemifusion, not complete fusion. Cell 1994;76: 383–391.
12. Haque ME, Chakraborty H, Koklic T, Komatsu H, Axelsen PH, Lentz BR. Hemagglutinin fusion peptide mutants in model membranes: structural properties, membrane physical properties, and PEG-mediated fusion. Biophys J 2011;101:1095–1104.
13. Huang Q, Chen CL, Herrmann A. Bilayer conformation of fusion peptide of influenza virus hemagglutinin: a molecular dynamics simulation study. Biophys J 2004;87:14–22.
14. Lagüe P, Roux B, Pastor RW. Molecular dynamics simulations of the influenza hemagglutinin fusion peptide in micelles and bilayers: conformational analysis of peptide and lipids. J Mol Biol 2005;354:1129–1141.
15. Li J, Das P, Zhou R. Single Mutation effects on conformational change and membrane deformation of influenza hemagglutinin fusion peptides. J Phys Chem B 2010;114:8799–8806.
16. Epand RM, Epand RF. Modulation of membrane curvature by peptides. Biopolymers 2000;55:358–363.
17. Gray C, Tamm LK. pH-Induced conformational changes of membrane-bound influenza hemagglutinin and its effect on target lipid bilayers. Protein Sci 1998;7:2359–2373.
18. Han X, Steinhauer DA, Wharton SA, Tamm LK. Interaction of mutant influenza virus hemagglutinin fusion peptides with lipid bilayers: probing the role of hydrophobic residue size in the central region of the fusion peptide. Biochemistry 1999;38:15052–15059.
19. Ge M, Freed JH. Fusion peptide from influenza hemagglutinin increases membrane surface order: an electron-spin resonance study. Biophys J 2009;96:4925–4934.
20. Kozlovsky Y, Zimmerberg J, Kozlov MM. Orientation and interaction of oblique cylindrical inclusions embedded in a lipid monolayer: a theoretical model for viral fusion peptides. Biophys J 2004; 87:999–1012.
21. Smirnova YG, Marrink S-J, Lipowsky R, Knecht V. Solvent-exposed tails as prestalk transition states for membrane fusion at low hydration. J Am Chem Soc 2010;132:6710–6718.
22. Stevens MJ, Hoh JH, Woolf TB. Insights into the molecular mechanism of membrane fusion from simulation: evidence for the association of splayed tails. Phys Rev Lett 2003;91:188102.
23. Mirjanian D, Dickey AN, Hoh JH, Woolf TB, Stevens MJ. Splaying of aliphatic tails plays a central role in barrier crossing during liposome Fusion. J Phys Chem B 2010;114:11061–11068.
24. Kasson PM, Lindahl E, Pande VS. Atomic-resolution simulations predict a transition state for vesicle fusion defined by contact of a few lipid tails. PLoS Comput Biol 2010;6:e1000829.
25. Larsson P, Kasson PM. Lipid tail protrusion in simulations predicts fusogenic activity of influenza fusion peptide mutants and conformational models. PLoS Comput Biol 2013;9:e1002950.
26. Epand RM, Epand RF, Richardson CD, Yeagle PL. Structural requirements for the inhibition of membrane-fusion by carbobenzoxy-D-Phe-Phe-Gly. Biochim Biophys Acta 1993;1152:128–134.

27. Teissier E, Zandomeneghi G, Loquet A, Lavillette D, Lavergne J-P, Montserret R, Cosset F-L, Boeckmann A, Meier BH, Penin F, Pécheur E-I. Mechanism of inhibition of enveloped virus membrane fusion by the antiviral drug arbidol. PLoS One 2011;6:e15874.
28. Colpitts CC, Ustinov AV, Epand RF, Epand RM, Korshun VA, Schang LM. 5-(perylen-3-yl) ethynyl-arabino-uridine (auy11), an arabino-based rigid amphipathic fusion inhibitor, targets virion envelope lipids to inhibit fusion of influenza virus, hepatitis c virus, and other enveloped viruses. J Virol 2013;87:3640–3654.
29. Lai AL, Park H, White JM, Tamm LK. Fusion peptide of influenza hemagglutinin requires a fixed angle boomerang structure for activity. J Biol Chem 2006;281:5760–5770.
30. Lai AL, Tamm LK. Locking the kink in the influenza hemagglutinin fusion domain structure. J Biol Chem 2007;282:23946–23956.
31. Charloteaux B, Lorin A, Brasseur R, Lins L. The "tilted peptide theory" links membrane insertion properties and fusogenicity of viral fusion peptides. Protein Pept Lett 2009;16:718–725.
32. Légaré S, Lagüe P. The influenza fusion peptide adopts a flexible flat V conformation in membranes. Biophys J 2012;102:2270–2278.
33. Han X, Bushweller JH, Cafiso DS, Tamm LK. Membrane structure and fusion-triggering conformational change of the fusion domain from influenza hemagglutinin. Nat Struct Biol 2001;8:715–720.
34. Brooks BR, Brooks CL, III, Mackerell AD, Jr., Nilsson L, Petrella RJ, Roux B, Won Y, Archontis G, Bartels C, Boresch S, Caflisch A, Caves L, Cui Q, Dinner AR, Feig M, Fischer S, Gao J, Hodoscek M, Im W, Kuczera K, Lazaridis T, Ma J, Ovchinnikov V, Paci E, Pastor RW, Post CB, Pu JZ, Schaefer M, Tidor B, Venable RM, Woodcock HL, Wu X, Yang W, York DM, Karplus M. CHARMM: the biomolecular simulation program. J Comput Chem 2009;30:1545–1614.
35. Bernèche S, Nina M, Roux B. Molecular dynamics simulation of melittin in a dimyristoylphosphatidylcholine bilayer membrane. Biophys J 1998;75:1603–1618.
36. Woolf TB, Roux B. Structure, energetics, and dynamics of lipid-protein interactions: a molecular dynamics study of the gramicidin A channel in a DMPC bilayer. Proteins 1996;24:92–114.
37. Allen TW, Andersen OS, Roux B. Structure of gramicidin A in a lipid bilayer environment determined using molecular dynamics simulations and solid-state NMR data. J Am Chem Soc 2003;125:9868–9877.
38. Phillips JC, Braun R, Wang W, Gumbart J, Tajkhorshid E, Villa E, Chipot C, Skeel RD, Kale L, Schulten K. Scalable molecular dynamics with NAMD. J Comput Chem 2005;26:1781–1802.
39. Feller SE, MacKerell AD. An improved empirical potential energy function for molecular simulations of phospholipids. J Phys Chem B 2000;104:7510–7515.
40. MacKerell AD, Feig M, Brooks CL. Extending the treatment of backbone energetics in protein force fields: limitations of gas-phase quantum mechanics in reproducing protein conformational distributions in molecular dynamics simulations. J Comput Chem 2004;25:1400–1415.
41. Jorgensen WL, Chandrasekhar J, Madura JD, Impey RW, Klein ML. Comparison of simple potential functions for simulating liquid water. J Chem Phys 1983;79:926–935.
42. Durell SR, Brooks BR, Ben-Naim A. Solvent-induced forces between 2 hydrophilic groups. J Phys Chem 1994;98:2198–2202.
43. Macias AT, MacKerell AD. CH/π interactions involving aromatic amino acids: refinement of the CHARMM tryptophan force field. J Comput Chem 2005;26:1452–1463.
44. Li L, Vorobyov I, Allen TW. The different interactions of lysine and arginine side chains with lipid membranes. J Phys Chem B 2013;117:11906–11920.
45. Su Y, Li S, Hong M. Cationic membrane peptides: atomic-level insight of structure-activity relationships from solid-state NMR. Amino Acids 2013;44:821–833.
46. Tang M, Waring AJ, Hong M. Phosphate-mediated arginine insertion into lipid membranes and pore formation by a cationic membrane peptide from solid-state NMR. J Am Chem Soc 2007;129:11438–11446.
47. Su Y, Doherty T, Waring AJ, Ruchala P, Hong M. Roles of arginine and lysine residues in the translocation of a cell-penetrating peptide from 13 C, 31 P, and 19 F solid-state NMR. Biochemistry 2009;48:4587–4595.
48. Li YL, Han X, Lai AL, Bushweller JH, Cafiso DS, Tamm LK. Membrane structures of the hemifusion-inducing fusion peptide mutant G1S and the fusion-blocking mutant G1V of influenza virus hemagglutinin suggest a mechanism for pore opening in membrane fusion. J Virol 2005;79:12065–12076.
49. Wishart DS, Sykes BD, Richards FM. Relationship between nuclear magnetic resonance chemical shift and protein secondary structure. J Mol Biol 1991;222:311–333.
50. Kates M, Tyrrell DAJ, James AT, Allison AC. Lipids of influenza virus and their relation to those of host cell. Biochim Biophys Acta 1961;52:455–466.
51. Yao H, Hong M. Membrane-dependent conformation, dynamics, and lipid interactions of the fusion peptide of the paramyxovirus PIV5 from solid-state NMR. J Mol Biol 2013;425:563–576.
52. Esbjorner EK, Oglecka K, Lincoln P, Graslund A, Norden B. Membrane binding of pH-sensitive influenza fusion peptides. Positioning, configuration, and induced leakage in a lipid vesicle model. Biochemistry 2007;46:13490–13504.
53. Lee D-K, Brender JR, Sciacca MFM, Krishnamoorthy J, Yu C, Ramamoorthy A. Lipid composition-dependent membrane fragmentation and pore-forming mechanisms of membrane disruption by pexiganan (MSI-78). Biochemistry 2013;52:3254–3263.
54. Wildman KAH, Lee DK, Ramamoorthy A. Mechanism of lipid bilayer disruption by the human antimicrobial peptide, LL-37. Biochemistry 2003;42:6545–6558.
55. Hallock KJ, Lee DK, Omnaas J, Mosberg HI, Ramamoorthy A. Membrane composition determines pardaxin's mechanism of lipid bilayer disruption. Biophys J 2002;83:1004–1013.
56. de Planque MRR, Boots JWP, Rijkers DTS, Liskamp RMJ, Greathouse DV, Killian JA. The effects of hydrophobic mismatch between phosphatidylcholine bilayers and transmembrane alpha-helical peptides depend on the nature of interfacially exposed aromatic and charged residues. Biochemistry 2002;41:8396–8404.
57. MacCallum JL, Bennett WFD, Tieleman DP. Distribution of amino acids in a lipid bilayer from computer simulations. Biophys J 2008;94:3393–3404.
58. Steinhauer DA, Wharton SA, Skehel JJ, Wiley DC. Studies of the membrane fusion activities of fusion peptide mutants of influenza virus hemagglutinin. J Virol 1995;69:6643–6651.
59. Qiao H, Armstrong RT, Melikyan GB, Cohen FS, White JM. A specific point mutant at position 1 of the influenza hemagglutinin fusion peptide displays a hemifusion phenotype. Mol Biol Cell 1999;10:2759–2769.
60. Markin VS, Kozlov MM, Borovjagin VL. On the theory of membrane fusion—the stalk mechanism. Gen Physiol Biophys 1984;3:361–377.
61. Siegel DP. Energetics of intermediates in membrane-fusion—comparison of stalk and inverted micellar intermediate mechanisms. Biophys J 1993;65:2124–2140.
62. Chernomordik LV, Frolov VA, Leikina E, Bronk P, Zimmerberg J. The pathway of membrane fusion catalyzed by influenza hemagglutinin: restriction of lipids, hemifusion, and lipidic fusion pore formation. J Cell Biol 1998;140:1369–1382.
63. Israelachvili JN. Intermolecular and Surface Forces, Revised 3rd ed. Waltham, MA: Academic Press; 2011. 704 p.
64. Israelachvili J, Wennerström H. Role of hydration and water structure in biological and colloidal interactions. Nature 1996;379:219–225.
65. Lagüe P, Zuckermann MJ, Roux B. Lipid-mediated interactions between intrinsic membrane proteins: dependence on protein size and lipid composition. Biophys J 2001;81:276–284.